RSC Chemical Biology

ROYAL SOCIETY OF CHEMISTRY

PAPER

View Article Online
View Journal | View Issue

Cite this: *RSC Chem. Biol.*, 2025, **6**, 754

Real-time bioluminescence imaging of nitroreductase in breast cancer bone metastasis†

Kang Lu,[a] Mengxi Zhang,[a] Zuotong Tian[a] and Han Xiao *[abcd]

Received 13th December 2024,
Accepted 13th March 2025

DOI: 10.1039/d4cb00310a

rsc.li/rsc-chembio

Bone metastasis is a leading cause of mortality in breast cancer patients. Monitoring biomarkers for bone metastasis in breast cancer is crucial for the development of effective interventional treatments. Despite being a highly vascularized tissue, the bone presents a particularly hypoxic environment. Tumor hypoxia is closely linked to increased levels of various reductases, including nitroreductase (NTR). Currently, there are few probes available to detect NTR levels in breast cancer bone metastases. Although bioluminescent imaging is promising due to its specificity and high signal-to-noise ratio, many probes face challenges such as short emission wavelengths, reliance on complex conditions like external adenosine triphosphate, or lack of tissue specificity. In this study, through "caging" the luciferase substrate with an NTR-responsive aromatic nitro recognition group, we developed a highly sensitive and selective NTR-sensitive bioluminescent probe. The resulting probe effectively detects NTR in breast cancer cells and enables real-time monitoring of NTR in a mouse model of breast cancer bone metastasis. Additionally, it can differentiate between primary and bone tumors, and allow continuous monitoring of NTR levels, thus providing valuable insights into bone tumor progression. This work provides a powerful tool for further understanding the biological functions of NTR in breast cancer bone metastasis.

Introduction

Breast cancer is the most common malignant tumor in women worldwide, with distant metastasis responsible for 90% of related deaths.[1,2] The bone is the most frequent site of metastasis, affecting 60% to 75% of patients with metastatic breast cancer.[3,4] Early treatment of primary tumors can often cure the disease, but once it metastasizes to the bones, the prognosis worsens.[5,6] Bone metastasis leads to severe pain, fractures, and complications that significantly reduce quality of life and survival.[7] Early and accurate detection is crucial for providing effective and personalized treatment options. The most common imaging technique for bone metastasis is ^{99m}Tc-methylene diphosphonate (^{99m}Tc-MDP), known for its cost-effectiveness and high sensitivity but limited by its lack of specificity and low spatial resolution.[8] Other imaging methods, such as positron emission tomography (PET), single photon emission computed tomography (SPECT), and magnetic resonance imaging (MRI), also have limitations in sensitivity, specificity, and safety.[9,10] Therefore, molecular imaging using biomarkers associated with tumor invasiveness and metastasis has emerged as a promising approach for the detection of bone metastasis in breast cancer.

Hypoxia, characterized by reduced tissue oxygen levels, is a hallmark of solid tumors.[11] It arises from a mismatch between increased oxygen consumption due to rapid tumor growth and inadequate oxygen supply caused by microvascular abnormalities.[12] Hypoxia is present in conditions such as stroke,[13] inflammation,[14] and vascular ischemia.[15] Notably, recent studies indicate that bone lesions in breast cancer metastases are particularly hypoxic than the primary tumors.[16,17] Assessing hypoxia in bone lesions is crucial for understanding metastatic behavior, as it triggers intracellular reductive stress and promotes the overexpression of reductases, such as nitroreductase (NTR).[18] NTR, a highly selective flavin mononucleotide (FMN)-dependent enzyme, serves as a promising hypoxia biomarker.[19–21] In human, NTR is often carried out by several different reductases such as cytochrome P450 reductase (CPR), NAD(P)H:quinone oxidoreductase 1 (NQO1), and others.[22–26] However, despite the critical role of NTR in hypoxic bone lesions, there are currently few molecular imaging tools available to monitor its high expression during breast cancer bone metastasis.

[a] *Department of Chemistry, Rice University, 6100 Main Street, Houston, TX, 77005, USA. E-mail: han.xiao@rice.edu*
[b] *SynthX Center, Rice University, 6100 Main Street, Houston, TX, 77005, USA*
[c] *Department of Biosciences, Rice University, 6100 Main Street, Houston, TX, 77005, USA*
[d] *Department of Bioengineering, Rice University, 6100 Main Street, Houston, TX, 77005, USA*

† Electronic supplementary information (ESI) available. See DOI: https://doi.org/10.1039/d4cb00310a

Unlike fluorescent imaging, bioluminescence imaging relies on the chemical reaction between luciferase and its substrate, luciferin, providing a high signal-to-noise ratio for specific imaging detection.[27–32] By genetically encoding luciferin in specific cells or tissues, light can be generated in a targeted manner. Previous studies have utilized ''caging'' strategy to temporarily block the luciferin–luciferase reaction, which is restored in the presence of specific analytes, such as enzymes, and some chemicals, producing a detectable photoluminescence.[33] Firefly luciferase (FLuc) is a common luciferase. However, the ATP-dependence of the FLuc system makes it susceptible to cellular ATP levels. In contrast, marine luciferases like Renilla luciferase (RLuc) are ATP-independent, making them more suitable for *in vivo* imaging. Recently, researchers have developed marine luciferase variants with higher catalytic activity and stability, such as NanoLuc luciferase (NLuc)-furimazine (FRZ).[34] Despite progress, the short-wavelength blue emission ($\sim$ 450 nm) of the NLuc-FRZ pair limits its widespread application for *in vivo* studies. To address this, researchers have developed a red-shifted substrate variant luciferin-QTZ, enabling emission at 585 nm.[35,36] This NLuc-QTZ system offers advantages like ATP-independence, high stability, and red-shifted emission, making it ideal for tumor imaging in xenograft mouse models. Based on this, we designed a bioluminescent probe for detecting NTR in breast cancer bone metastasis. Specifically, we developed a NTR-responsive probe with a specific aromatic nitro group, conjugated to the carbonyl group of QTZ. In the presence of NTR, this ''caged'' luciferin undergoes a self-cleavage process and generate QTZ, which can be catalyzed by NLuc to produce bioluminescence. QTZ-NTR selectively detects NTR with a low detection limit and shows promise for monitoring NTR in living cells and a mouse model of breast cancer bone metastasis.

Results and discussion

Design and characterization of bioluminescence NTR probe

The reported QTZ exhibits several key advantages, including enhanced luminescence redshift for superior deep-tissue imaging when paired with NLuc. Additionally, it features a compact size, excellent stability, and high reactivity, making it a versatile tool for advanced imaging applications.[37] Despite these advantages, researchers are actively developing new platforms to enhance QTZ's responsiveness to specific analytes, thereby broadening its range of applications. A widely used approach involves stabilizing the QTZ with chemical protective groups, creating a ''caged'' structure. Upon interaction with specific targets, such as enzymes or biomolecules, these protective groups are cleaved, converting the ''caged'' substrate into its active form and triggering bioluminescence.[38–40]

To develop a NTR-responsive bioluminescent probe for the NLuc-QTZ system, we modified QTZ by attaching NTR-recognition moiety. The aromatic nitro group is expected to specifically react with NTR, triggering an electron cascade to reveal the parent QTZ.[21] The synthesis of QTZ begins with 5-bromo-3-iodopyrazine-2-amine as the starting material, followed by two Suzuki coupling reactions to form the key pyrazine core (5-phenyl-3-(quinolin-4-yl)pyrazine-2-amine), which is then condensed with a dioxy derivative in ethanol and concentrated HCl to generate QTZ. To verify the effectiveness of the recognition groups and their ''caging'' ability on the luciferin QTZ, we also synthesized a control compound, QTZ-control, using benzyl bromide (Fig. 1A). Detailed synthesis steps and characterization are provided in the ESI.†

In vitro evaluation of QTZ-NTR towards NTR

We investigated the reactivity of QTZ-NTR towards NTR in PBS buffer (pH 7.4, 10 mM). As shown in Fig. 1B and C, the time- and concentration-dependent luminescence spectra indicated that in the absence of NTR, QTZ-NTR showed minimal bioluminescence. However, as the NTR concentration increased, the luminescence of QTZ-NTR (10 μM) progressively augmented. Specifically, the addition of 10 μg mL^{-1} NTR induced a rapid increase in luminescence by approximately 40 times within 20 minutes. The bioluminescence intensity exhibited a linear correlation with NTR concentration in the range of 0 to 1.5 μg mL^{-1}, and the detection limit (Signal-to-noise ratio, S/N = 3) of QTZ-NTR for NTR was 0.051 μg mL^{-1} (Fig. 1E). In contrast, QTZ-control showed no significant reaction with NTR, yielding almost no luminescent signal (Fig. 1D). These results demonstrate that QTZ-NTR can detect NTR rapidly and sensitively. Furthermore, HR-MS analysis confirmed the production of QTZ. The reaction product, with an MS peak of *m/z* $[M+H]^+$ = 429.1749 (Fig. S1, ESI†), was identified as QTZ ($[M+H]^+$ calculated for $C_{28}H_{21}N_4O$: 429.1715), consistent with the proposed NTR-reduced cleavage mechanism (Fig. 1A and Scheme S1, ESI†). NTR facilitates electron transfer *via* FMN, with NAD(P)H serving as the electron donor to reduce the nitro substrate. A single reduction cycle yields hydroxylamine, while a second cycle produces an amine, finally leading to QTZ formation, which emits light under NLuc.[35,41]

Evaluating the response of QTZ-NTR towards different analytes in complex environments is essential for assessing its activity and specificity for NTR detection.[42] In selectivity tests, a variety of related substances were tested, including reducing thiols (Cys and GSH), arginine (Arg), ascorbic acid, reactive oxygen, nitrogen, and sulfur-containing species (NO, CO, SO_3^{2-}, SH^-, and $S_2O_3^{2-}$), and inorganic cations (Ca^{2+}, K^+, Zn^{2+}, Hg^{2+}, Fe^{2+} and Mg^{2+}). NADPH was used as the electron donor in the reduction process. In the absence of NTR or reducing agents, no significant luminescence enhancement was observed (Fig. 1F). However, when both NTR (10 μg mL^{-1}) and NADPH (0.1 mM) were present, luminescence increased more than threefold compared to other biologically relevant substances. A slight increase in luminescence occurred when either NTR or NADPH was tested alone, confirming that both the enzyme and NADPH are necessary for bioluminescence. These results demonstrate that QTZ-NTR selectively detects NTR without interference from other analytes.

To further understand the relationship between structure of QTZ-NTR and NTR/NADPH, we conducted docking calculations.[43,44] The formation of hydrogen bonds between the substrate and NTR is a

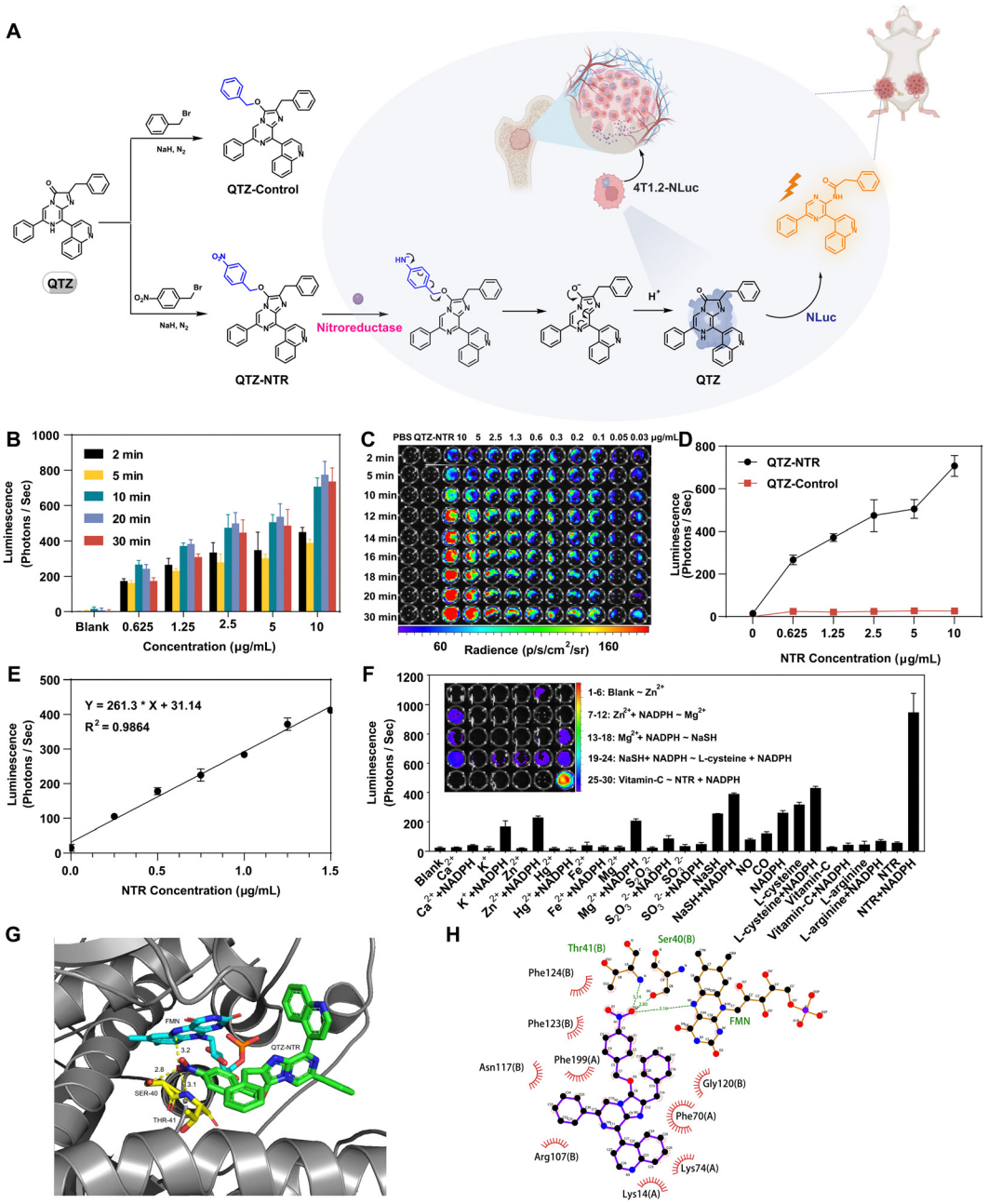

Fig. 1 (A) The synthetic route and the NTR-responsive bioluminescent probe QTZ-NTR and QTZ-control; (B) bioluminescent response of QTZ-NTR (100 μM) when treated with increased NTR concentrations, NADPH (0.1 mM) and NLuc (0.5 μg mL^{-1}) in PBS buffer (10 mM, pH 7.4) for a different incubation time at 37 °C; (C) relative bioluminescence images in a 96-well black plate after treating QTZ-NTR (100 μM) with NTR (0.03–10 μg mL^{-1}), NADPH (0.1 mM), and NLuc (0.5 μg mL^{-1}) in PBS buffer (10 mM, pH 7.4) for a different incubation time at 37 °C; (D) comparison of the luminescent reactivity of QTZ-NTR and QTZ-control (100 μM) with different concentrations of NTR, NADPH (0.1 mM) and 0.5 μg mL^{-1} NLuc in PBS buffer (pH 7.4, 10 mM) after incubation at 37 °C for 30 minutes; (E) concentration-dependent luminescence changes of QTZ-NTR after incubation with NTR, NADPH (0.1 mM) and 0.5 μg mL^{-1} NLuc for 30 min. The linear relationship is described as $y = 261.3\,x + 31.14$ ($R^2 = 0.9864$), and the linearity range of NTR is from 0.25 μg mL^{-1} to 1.5 μg mL^{-1}; (F) Bioluminescence responses of QTZ-NTR (100 μM) toward different analytes in PBS buffer (pH 7.4, 10 mM) after incubation at 37 °C for 30 minutes: blank, Ca^{2+}(10 mM), Ca^{2+} + NADPH (10 mM, 0.1 mM), K^{+}(10 mM), K^{+} + NADPH (10 mM, 0.1 mM), Zn^{2+} (10 mM), Zn^{2+} + NADPH (10 mM, 0.1 mM), Hg^{2+} (10 mM), Hg^{2+} + NADPH(10 mM, 0.1 mM), Fe^{2+} (10 mM), Fe^{2+} + NADPH (10 mM, 0.1 mM), Mg^{2+}(10 mM), Mg^{2+} + NADPH (10 mM, 0.1 mM), $S_2O_3^{2-}$(1 mM), $S_2O_3^{2-}$ + NADPH (1 mM, 0.1 mM), SO_3^{2-}(1 mM), SO_3^{2-} + NADPH (1 mM, 0.1 mM), SH^{-} (1 mM), SH^{-} + NADPH (1 mM, 0.1 mM), NO (0.5 mM), CO (0.5 mM), NADPH (0.5 mM), L-cysteine (1 mM), L-cysteine + NADPH (1 mM, 0.1 mM), vitamin C (1 mM), vitamin C + NADPH (1 mM, 0.1 mM), L-arginine (1 mM), L-arginine + NADPH (1 mM, 0.1 mM), NTR (10 μg mL^{-1}), and NTR + NADPH (10 μg mL^{-1}, 0.1 mM). Data are presented as mean ± SD ($n = 3$); Calculated binding model of QTZ-NTR (G) and (H) with NTR. In (G), the C, N, and O atoms of QTZ-NTR structure are shown in green, blue, and red, respectively; In (H), the C, N, and O atoms of QTZ-NTR are shown in black, blue, and red, respectively. Red curves are indicated the hydrophobic areas and the amino acid residues of the NTR. Hydrogen bonds are indicated with green dotted lines. PDB: 4DN2.

key step in the catalytic process. As shown in Fig. 1G and H, QTZ-NTR tends to approach the hydrophobic pocket of NTR through hydrophobic interactions and aromatic π–π interactions. The transition state is then formed *via* three hydrogen bonds between the amino acid residue Ser40, Thr41, the cofactor FMN of NTR and the oxygen atom of nitro in QTZ-NTR. These results highlight the strong linkage between the detection moiety and luminescent reporter, and explain why QTZ-NTR shows high reactivity and sensitivity towards NTR/NADPH.

Bioluminescence imaging of intracellular NTR

Next, we evaluated the capability of QTZ-NTR to detect NTR level in living cells. 4T1.2 cell, commonly used in breast cancer bone metastasis research, was employed in this study.[45,46] First, we used lentivirus-mediated transfection and clonal single-cell proliferation techniques to successfully introduce NLuc into 4T1.2 cells, creating a stable 4T1.2-NLuc cell line. Detailed experiments are provided in the ESI.† Then we studied cytotoxicity of QTZ-NTR in 4T1.2-NLuc cells. Results showed low cytotoxicity with cell viability over 75% at 500 μM, indicating its good compatibility and suitability for cell imaging (Fig. S7, ESI†). To test QTZ-NTR's ability to detect NTR in living cells, we first stimulated 4T1.2-NLuc cells with cobalt chloride ($CoCl_2$) to elevate NTR levels.[47,48] Bioluminescence intensity increased steadily with increasing concentration of $CoCl_2$ (0 – 62.5 μM), demonstrating that QTZ-NTR can monitor dynamic changes of NTR levels in 4T1.2-NLuc cells (Fig. 2A). At higher $CoCl_2$ concentrations, bioluminescence signals decreased due to the cytotoxic effects of $CoCl_2$ (Fig. 2A and Fig. S3, ESI†). Then we used the coverslip method to evaluate the hypoxia-induced upregulation of NTR in 4T1.2-NLuc cells.[49] In this approach, a glass coverslip was placed over the cultured cells to create a localized hypoxic microenvironment by limiting oxygen transport and consumption (Fig. 2C). After 1 hour of hypoxia, QTZ-NTR-treated cells exhibited increased luminescence compared to those under normoxic conditions (Fig. 2D), demonstrating that QTZ-NTR effectively detects NTR expression in hypoxia. Next, we investigated QTZ-NTR's ability to monitor endogenous NTR without external stimuli. After incubation with 62.5 μM QTZ-NTR for 20 min, 4T1.2-NLuc cells showed strong bioluminescence, correlating with high NTR expression in breast cancer cells. Bioluminescence intensity increased with cell density (Fig. 2E). These results suggest that QTZ-NTR is effective for monitoring NTR in 4T1.2-NLuc cells. Finally, to assess whether endogenous NTR triggers bioluminescence, we pretreated 4T1.2-NLuc cells with the NTR inhibitor dicoumarol.[50] After 30 minutes, cells were incubated with 10 μM QTZ-NTR for bioluminescence imaging. As shown in Fig. 2G and H, dicoumarol-treated cells exhibited significantly reduced bioluminescence compared to untreated cells ($P < 0.0001$). These results confirm that QTZ-NTR is a sensitive and specific probe for detecting NTR expression in cancer cells.

In vivo bioluminescence imaging of breast cancer bone metastasis using QTZ-NTR

After confirming that QTZ-NTR exhibited excellent bioluminescence response in aqueous solution and cells, we explored whether this probe could serve as a reporter for the NTR level of bone metastatic niche *in vivo*. A breast cancer bone metastatic model was established in Balb/c mice by injecting 4T1.2-NLuc cells into the left tibia, while simultaneously injecting the cells into the right mammary fat pad to create an orthotopic breast primary tumor as control.[51–53] QTZ-NTR was intravenously injected into the mice bearing both the primary and

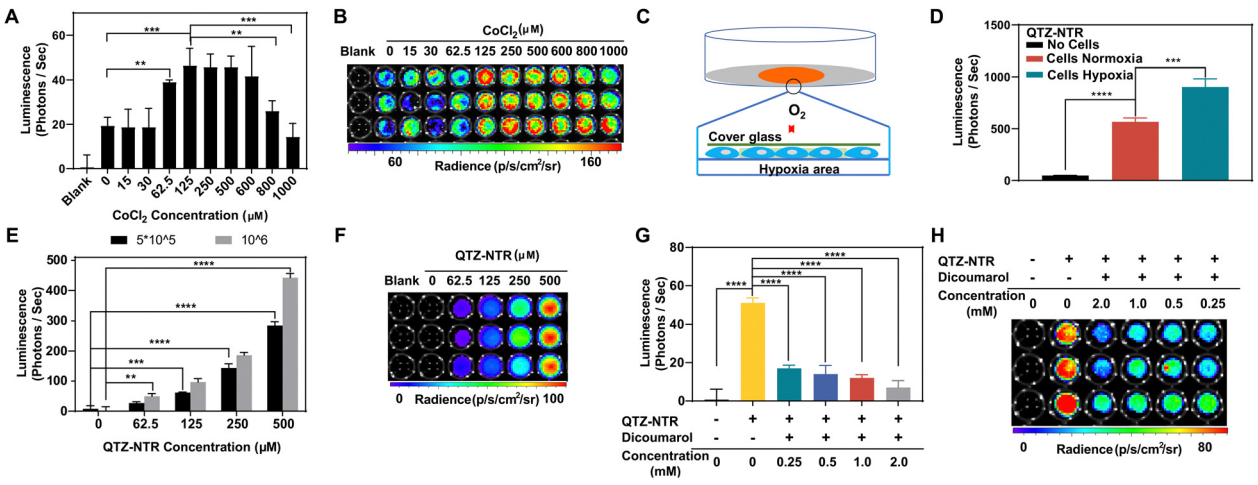

Fig. 2 (A) Bioluminescent response of QTZ-NTR (100 μM) when treated with increased $CoCl_2$ concentrations in 4T1.2-NLuc cells for 30 min at 37 °C; (B) Representative bioluminescence images of (A) shown in 96-well black plates; (C) graphical description of the establishment of local cellular hypoxia by placing a glass coverslip on top of the cells for 1 h; (D) bioluminescence imaging of NTR in hypoxic 4T1-NLuc cells: 4T1-NLuc cells were subjected to hypoxic incubation for 1 h and incubated with QTZ-NTR at 37 °C for 10 min, then imaged; (E) bioluminescent response of NTR in 5×10^5 and 1×10^6 4T1.2-NLuc cells per mL toward different concentration QTZ-NTR (0 μM, 62.5 μM, 125 μM, 250 μM, and 500 μM) at 37 °C; (F) representative bioluminescence images of (E) shown in 96-well black plates; (G) inhibition effect of different concentration of dicoumarol on NTR production in 4T1.2-NLuc cells; (H) representative bioluminescence images of (G) shown in 96-well black plates. Data are presented as mean ± SD ($n = 3$). *P* values were determined by one-way ANOVA with Tukey's multiple comparisons test. $^{**}p < 0.01$, $^{***}p < 0.001$, $^{****}p < 0.0001$.

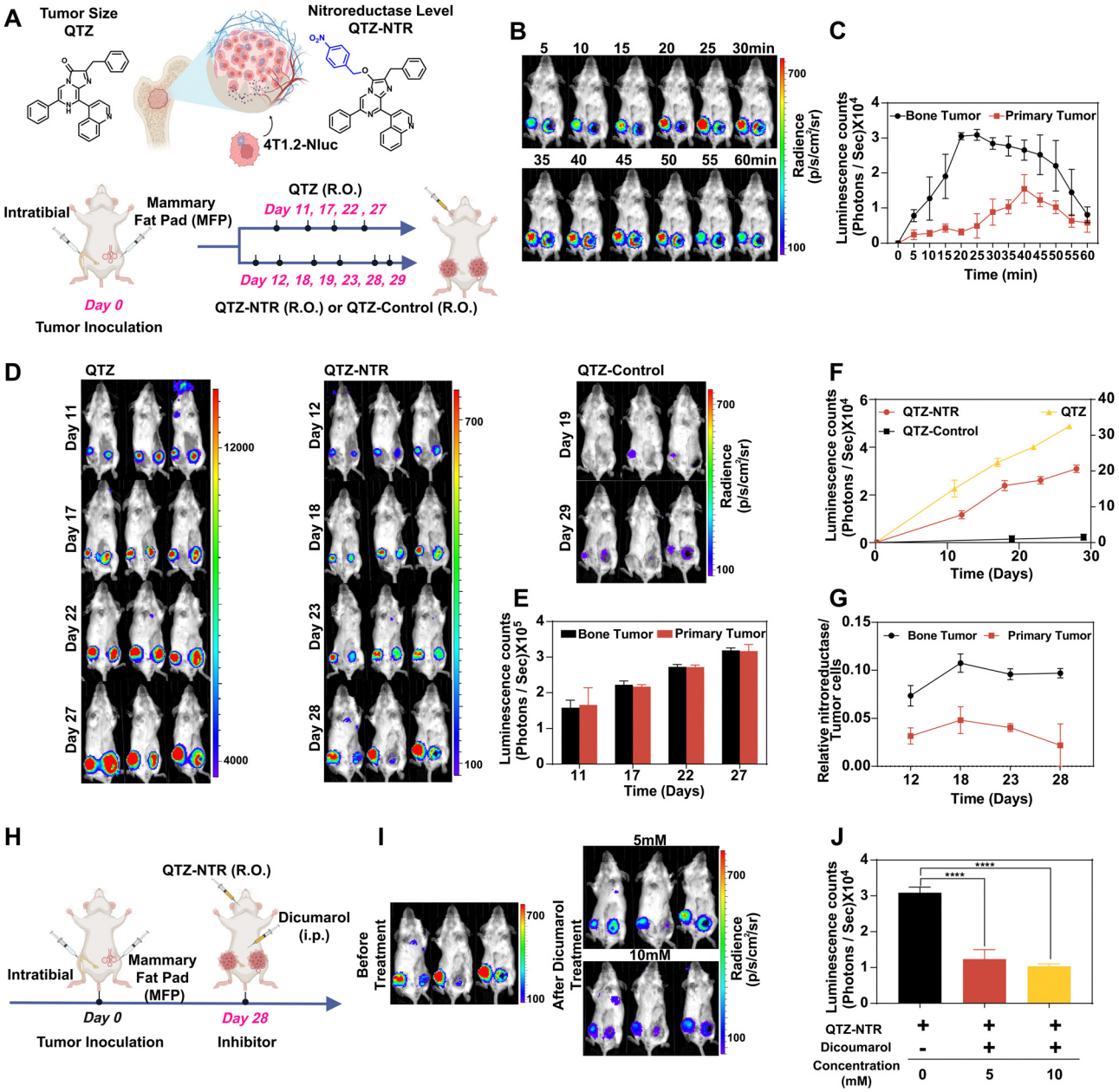

Fig. 3 (A) Schematic illustrations of roles for two luminescent substrates (QTZ-NTR and QTZ) in breast cancer bone tumor detection and the treatments (using QTZ-NTR, QTZ, and QTZ-control) for 4T1.2-NLuc primary and bone metastatic tumor models; (B) bioluminescence imaging of NTR in 4T1.2-NLuc primary and bone metastatic tumor models. The mice were intravenously injected with QTZ-NTR (100 μL, 1 mM) on 28th day; (C) relative bioluminescence intensity of primary and bone metastatic tumor in (B); (D) tumor growth monitored using the luciferin substrate QTZ (100 μL, 1 mM) on days 11, 17, 22 and 27; fluctuations of NTR in the tumor monitored using QTZ-NTR (100 μL, 1 mM) on days 12, 18, 23 and 28, and QTZ-control (100 μL, 1 mM) on days 19 and 29 in 4T1.2-NLuc primary and bone metastatic tumor models. (E) Relative bioluminescence intensity of primary and bone metastatic tumors in the QTZ group in (D) at days 11, 17, 22, and 27; (F) Relative bioluminescence intensity of bone metastatic tumors in the QTZ-NTR group in (D) on days 12, 18, 23, and 28; (G) quantitative analysis (the ratio of bioluminescence intensity in the QTZ-NTR group to that in the QTZ group) of NTR expression in primary and bone metastatic tumors of the QTZ-NTR group in (D) on days 12, 18, 23, and 28; (H) schematic illustrations of the treatment (using inhibitor dicoumarol) for 4T1.2-NLuc primary and bone metastasis mouse model. (I) Bioluminescence imaging of NTR in 4T1.2-NLuc primary and bone metastatic tumor models. Mouse in the control group was intravenously injected with QTZ-NTR (100 μL, 1 mM), while mice in the inhibitor groups were intraperitoneally injected with dicoumarol (100 μL, 5 mM and 10 mM) then intravenously inject QTZ-NTR (100 μL, 1 mM). (J) Relative bioluminescence intensity in (I). Data are presented as mean ± SD (n = 3). P values were determined by one-way ANOVA with Tukey's multiple comparisons test. ****$p < 0.0001$.

bone metastatic tumor models, and bioluminescence imaging was performed (Fig. 3A). To determine the optimal imaging time, bioluminescence imaging was conducted at intervals from 5 to 60 minutes (Fig. 3B and C). The results showed that the luminescence intensity of the bone metastasis gradually increased, peaked at 25 minutes, and remained stable for about

5 minutes before decreasing due to depletion of QTZ-NTR. Therefore, 25 minutes was selected as the optimal time point for subsequent imaging to ensure maximum signal strength and image quality. Importantly, QTZ, an effective NLuc substrate, enables the detection of primary and bone metastatic tumor onset and progression, as demonstrated in our bioluminescence imaging studies. Furthermore, QTZ-NTR, with its sensitivity to NTR levels within hypoxic tumor microenvironments, allows for efficient detection of NTR expression in both tumor types. By comparing the bioluminescence signal ratio of QTZ-NTR to QTZ, we can quantitatively assess the progression of NTR expression, offering a comprehensive analysis of NTR dynamics in primary and bone metastatic tumors. To quantify fluctuations in NTR during tumor growth, QTZ and QTZ-NTR were alternately injected on different days. Tumor detection with QTZ at both sites revealed stable, similar signals for orthotopic and bone tumors, with comparable tumor growth (Fig. 3D and E). The bioluminescence intensity of both tumors injected with QTZ gradually increased on days 11, 17, 22, and 27, indicating similar growth patterns for orthotopic and bone metastatic tumors (Fig. 3D and E). However, after intravenous injection of QTZ-NTR, the bone tumor exhibited significantly stronger bioluminescence than the orthotopic breast cancer tumor, with the intensity increasing progressively on days 12, 18, 23, and 28 (Fig. 3D, F and G). These findings strongly suggest that QTZ-NTR can non-invasively and real-time monitor NTR levels during breast cancer bone metastasis, highlighting its potential as a valuable tool for assessing the hypoxic microenvironment of bone metastases. As a control, 4T1.2-NLuc primary and bone metastatic tumors-bearing mice injected with QTZ-control showed weak bioluminescence (Fig. 3D and F), confirming that QTZ-NTR is a powerful tool for detecting NTR in the bone tumor environment. Additionally, we evaluated the efficacy of enzyme inhibitors of NTR *in vivo* (Fig. 3H). After intraperitoneal injection of different concentrations of dicoumarol for 4 hours, bioluminescence inhibition in dicoumarol-pretreated mice was significantly lower than in the control group ($P < 0.0001$) (Fig. 3I and J). In summary, these results clearly demonstrate that QTZ-NTR can monitor NTR level during the bone tumor progression *in vivo*, providing a foundation for further investigation into the biological role of NTR in breast cancer bone metastasis.

Conclusions

In summary, we developed a novel bioluminescent imaging probe, QTZ-NTR, and first demonstrated its effectiveness in detecting NTR in breast cancer bone metastasis. Unlike other probes for NTR detection, the QTZ-NTR/NLuc system features a red-shifted emission wavelength for deep tissue imaging and does not require external ATP, thus simplifying experimental conditions. Moreover, QTZ-NTR exhibits good selectivity for NTR, with a detection limit of 0.051 μg mL^{-1} in PBS buffer. The probe successfully senses NTR in 4T1.2-NLuc cells. In a mouse model of breast cancer bone metastasis, QTZ-NTR not only effectively distinguishes primary tumors from bone metastatic tumors, indirectly reflecting the higher levels of hypoxia in bone tumor lesions, but also allows for the evaluation of dynamic changes in NTR expression during the development and progression of bone tumors. This bioluminescent imaging technique offers a valuable tool for studying the roles of NTR and hypoxia in bone tumor progression associated with breast cancer metastasis.

Ethical statement

All mouse protocols were in accordance with NIH guidelines and were approved by the Institutional Animal Care and Use Committee of Rice University.

Data availability

The data underlying this article are available in the article and in the ESI.†

Conflicts of interest

The authors declare no competing financial interest.

Acknowledgements

This work was supported by NIH (R01-CA277838, R35-GM133706, R21EB033607, and R01-AI165079 to H.X.), the Robert A. Welch Foundation (C-1970 to H.X.), US Department of Defense (HT9425-23-1-0494, HT94252510021, and W81XWH-21-1-0789 to H.X.), the Medical Research Award from Robert J. Kleberg, Jr. and Helen C. Kleberg Foundation (to H.X.), and the Hamill Innovation Award (to H.X.). H.X. is a Cancer Prevention & Research Institute of Texas (CPRIT) scholar in cancer research.

Notes and references

1 R. L. Siegel, K. D. Miller and A. Jemal, *Ca-Cancer J. Clin.*, 2019, **69**, 7–34.
2 C. L. Chaffer and R. A. Weinberg, *Science*, 2011, **331**, 1559–1564.
3 B. Weigelt, J. L. Peterse and L. J. Van'T Veer, *Nat. Rev. Cancer*, 2005, **5**, 591–602.
4 K. N. Weilbaecher, T. A. Guise and L. K. McCauley, *Nat. Rev. Cancer*, 2011, **11**, 411–425.
5 N. Harbeck, F. Penault-Llorca, J. Cortes, M. Gnant, N. Houssami, P. Poortmans, K. Ruddy, J. Tsang and F. Cardoso, *Nat. Rev. Dis. Primers*, 2019, **5**, 66.
6 Y. Wang, C. Wang, M. Xia, Z. Tian, J. Zhou, J. M. Berger, X. H.-F. Zhang and H. Xiao, *Mol. Ther.*, 2024, **32**, 1219–1237.
7 F. Macedo, K. Ladeira, F. Pinho, N. Saraiva, N. Bonito, L. Pinto and F. Gonçalves, *Oncol. Rev.*, 2017, **11**, 43–49.
8 P. Wu, D. J. Siegwart and H. Xiong, *Sci. China: Chem.*, 2021, **64**, 1283–1296.
9 R. S. Fernandes, D. Dos Santos Ferreira, C. De Aguiar Ferreira, F. Giammarile, D. Rubello and A. L. B. De Barros, *Biomed. Pharmacother.*, 2016, **83**, 1253–1264.

10 Q. Meng and Z. Li, *Int. J. Biomed. Imaging*, 2013, **2013**, 1–14.
11 A. L. Harris, *Nat. Rev. Cancer*, 2002, **2**, 38–47.
12 P. Vaupel, F. Kallinowski and P. Okunieff, *Cancer Res.*, 1989, **49**, 6449–6465.
13 S. Kizaka-Kondoh, M. Inoue, H. Harada and M. Hiraoka, *Cancer Sci.*, 2003, **94**, 1021–1028.
14 C. Murdoch, M. Muthana and C. E. Lewis, *J. Immunol.*, 2005, **175**, 6257–6263.
15 G. L. Semenza, *Annu. Rev. Med.*, 2003, **54**, 17–28.
16 H. Knowles, *Hypoxia*, 2015, 73.
17 V. M. Todd and R. W. Johnson, *Cancer Lett.*, 2020, **489**, 144–154.
18 J. M. Brown and W. R. Wilson, *Nat. Rev. Cancer*, 2004, **4**, 437–447.
19 H. Wang, M. Yang, M. Ji and P. Wang, *J. Photochem. Photobiol., A*, 2022, **427**, 113814.
20 S. Das, H. K. Indurthi, P. Asati and D. K. Sharma, *ChemistrySelect*, 2022, **7**, e202102895.
21 Y.-L. Qi, L. Guo, L.-L. Chen, H. Li, Y.-S. Yang, A.-Q. Jiang and H.-L. Zhu, *Coord. Chem. Rev.*, 2020, **421**, 213460.
22 C. P. Guise, A. T. Wang, A. Theil, D. J. Bridewell, W. R. Wilson and A. V. Patterson, *Biochem. Pharmacol.*, 2007, **74**, 810–820.
23 L. Miseviciene, Z. Anusevicius, J. Sarlauskas and N. Cenas, *Acta Biochim. Pol.*, 2006, **53**, 569–576.
24 J. J. Doel, B. L. J. Godber, T. A. Goult, R. Eisenthal and R. Harrison, *Biochem. Biophys. Res. Commun.*, 2000, **270**, 880–885.
25 E. M. Paragas, S. C. Humphreys, J. Min, C. A. Joswig-Jones and J. P. Jones, *Biochem. Pharmacol.*, 2017, **145**, 210–217.
26 G. E. Smyth and B. A. Orsi, *Biochem. J.*, 1989, **257**, 859–863.
27 A. J. Syed and J. C. Anderson, *Chem. Soc. Rev.*, 2021, **50**, 5668–5705.
28 J. Tang, M. A. Robichaux, K.-L. Wu, J. Pei, N. T. Nguyen, Y. Zhou, T. G. Wensel and H. Xiao, *J. Am. Chem. Soc.*, 2019, **141**, 14699–14706.
29 S. Wang, H. Shi, L. Wang, A. Loredo, S. M. Bachilo, W. Wu, Z. Tian, Y. Chen, R. B. Weisman, X. Zhang, Z. Cheng and H. Xiao, *J. Am. Chem. Soc.*, 2022, **144**, 23668–23676.
30 Y. Liu, C. H. Wolstenholme, G. C. Carter, H. Liu, H. Hu, L. S. Grainger, K. Miao, M. Fares, C. A. Hoelzel, H. P. Yennawar, G. Ning, M. Du, L. Bai, X. Li and X. Zhang, *J. Am. Chem. Soc.*, 2018, **140**, 7381–7384.
31 R. E. Wang, Y. Zhang, J. Cai, W. Cai and T. Gao, *Curr. Med. Chem.*, 2011, **18**, 4175–4184.
32 I. M. Mostafa, A. Abdussalam, Y. T. Zholudov, D. V. Snizhko, W. Zhang, M. Hosseini, Y. Guan and G. Xu, *Chem. Biomed. Imaging*, 2023, **1**, 297–314.
33 X. Yang, X. Qin, H. Ji, L. Du and M. Li, *Org. Biomol. Chem.*, 2022, **20**, 1360–1372.
34 X. Shi, Y. Wang, J. Yu, Y. Yang, Z. Jin, H. Wang, D. Wu, W. Chen, J. Guo and Y. Zhang, *Chin. J. Chem.*, 2024, **42**, 1373–1380.
35 Y. Xiong, Y. Zhang, Z. Li, M. S. Reza, X. Li, X. Tian and H. Ai, *J. Am. Chem. Soc.*, 2022, **144**, 14101–14111.
36 K. Lu, Y. Wang, C. Wang, R. Liu, K. Yang, X. Zhang and H. Xiao, *ACS Bio Med Chem Au*, 2025, **5**, 175–183.
37 M. P. Hall, J. Unch, B. F. Binkowski, M. P. Valley, B. L. Butler, M. G. Wood, P. Otto, K. Zimmerman, G. Vidugiris, T. Machleidt, M. B. Robers, H. A. Benink, C. T. Eggers, M. R. Slater, P. L. Meisenheimer, D. H. Klaubert, F. Fan, L. P. Encell and K. V. Wood, *ACS Chem. Biol.*, 2012, **7**, 1848–1857.
38 Y. Mizui, M. Eguchi, M. Tanaka, Y. Ikeda, H. Yoshimura, T. Ozawa, D. Citterio and Y. Hiruta, *Org. Biomol. Chem.*, 2021, **19**, 579–586.
39 E. Lindberg, S. Mizukami, K. Ibata, A. Miyawaki and K. Kikuchi, *Chem. – Eur. J.*, 2013, **19**, 14970–14976.
40 M. Orioka, M. Eguchi, Y. Mizui, Y. Ikeda, A. Sakama, Q. Li, H. Yoshimura, T. Ozawa, D. Citterio and Y. Hiruta, *Bioconjugate Chem.*, 2022, **33**, 496–504.
41 M. D. Roldán, E. Pérez-Reinado, F. Castillo and C. Moreno-Vivián, *FEMS Microbiol. Rev.*, 2008, **32**, 474–500.
42 K. Xu, F. Wang, X. Pan, R. Liu, J. Ma, F. Kong and B. Tang, *Chem. Commun.*, 2013, **49**, 2554.
43 S. Mirzaie, F. Rafii, K. Yasunaga, K. Yoshunaga, Z. Sepehrizadeh, S. Kanno, Y. Tonegawa and A. Reza Shahverdi, *Comput. Biol. Med.*, 2012, **42**, 414–421.
44 Y. Li, Y. Sun, J. Li, Q. Su, W. Yuan, Y. Dai, C. Han, Q. Wang, W. Feng and F. Li, *J. Am. Chem. Soc.*, 2015, **137**, 6407–6416.
45 K. Tawara, C. Bolin, J. Koncinsky, S. Kadaba, H. Covert, C. Sutherland, L. Bond, J. Kronz, J. R. Garbow and C. L. Jorcyk, *Breast Cancer Res.*, 2018, **20**, 53.
46 Y. Wang, Z. Xu, K.-L. Wu, L. Yu, C. Wang, H. Ding, Y. Gao, H. Sun, Y.-H. Wu, M. Xia, Y. Chen and H. Xiao, *Proc. Natl. Acad. Sci. U. S. A.*, 2024, **121**, e2312929121.
47 G. L. Semenza, *Cell*, 2001, **107**, 1–3.
48 R. L. Koder and A.-F. Miller, *Biochim. Biophys. Acta*, 1998, **1387**, 395–405.
49 J. Xiong, P. Wang, S. Son, C. Zhong, F. Zhang, Z. Mao, Z. Liu and J. S. Kim, *Matter*, 2022, **5**, 1502–1519.
50 E. Johansson, G. N. Parkinson, W. A. Denny and S. Neidle, *J. Med. Chem.*, 2003, **46**, 4009–4020.
51 H. I. Atiya, A. Dvorkin-Gheva, J. Hassell, S. Patel, R. L. Parker, A. Hartstone-Rose, J. Hodge, D. Fan and A. F. Ramsdell, *Anticancer Res.*, 2019, **39**, 2277–2287.
52 Z. Tian, C. Yu, W. Zhang, K.-L. Wu, C. Wang, R. Gupta, Z. Xu, L. Wu, Y. Chen, X. H.-F. Zhang and H. Xiao, *ACS Cent. Sci.*, 2022, **8**, 312–321.
53 Z. Tian, L. Wu, C. Yu, Y. Chen, Z. Xu, I. Bado, A. Loredo, L. Wang, H. Wang, K.-L. Wu, W. Zhang and H. Xiao, *Sci. Adv.*, 2021, **7**, eabf2051.